CrystEngComm

RSC Publishing

PAPER

View Article Online
View Journal | View Issue

Cite this: *CrystEngComm*, 2013, **15**, 6979

Distribution of thulium in Tm^{3+}-doped oxyfluoride glasses and glass-ceramics

A. de Pablos-Martin,*[ab] C. Patzig,[a] T. Höche,[a] A. Duran[b] and M. J. Pascual[b]

Received 26th April 2013,
Accepted 2nd July 2013

DOI: 10.1039/c3ce40731d

www.rsc.org/crystengcomm

Rare-earth (RE) doped transparent glass-ceramics are presented as very promising materials for optical applications. In this work, Transmission Electron Microscopy techniques have been used to structurally characterize a glass of composition $55SiO_2$–$20Al_2O_3$–$15Na_2O$–$10LaF_3$ (mol%), doped with 1 mol% Tm_2O_3, and the corresponding glass-ceramic. The proposed crystallization mechanism for this glass has been modified from the results obtained through advanced STEM/EDXS techniques. The parent glass contains phase separated regions mainly enriched in F and La and also in Al, Si and Tm. After annealing, 10–20 nm LaF_3 nano-crystals are formed from these phase separated droplets. The partial incorporation of the doping Tm^{3+} ions into the LaF_3 nano-crystals has been verified and the interphase crystal/glassy matrix has been more precisely characterized through EDXS. An Al enriched layer is formed around the crystals followed by a Si enriched shell, which greatly increase the viscosity in the periphery of the crystals, inhibiting further crystal growth and thus, keeping the nano size of the crystals.

Introduction

The synthesis of rare-earth (RE) ion-doped oxyfluoride glass-ceramics is a promising way to obtain crystalline phases with very low phonon energies, like LaF_3,[1] $NaLaF_4$,[2] and $NaYF_4$,[3] embedded in a glassy matrix. In such transparent materials, the crystal phases act as hosts for the RE ions, thus enhancing radiative optical-emission processes, like up- and down-conversion emissions,[4] yet still keeping the good mechanical properties of silicate matrices.

Rüssel[5] proposed a mechanism of inhibition of crystal growth, based in CaF_2 crystallizing oxyfluoride glasses, in which the remaining glassy matrix is enriched in network formers after crystallization, leading to an increase in viscosity, which inhibits the further crystal growth and enables to maintain nano-size crystals. Later, it was reported from TEM techniques the formation of a silicon barrier around the precipitated BaF_2 nano-crystals in the oxyfluoride glass studied in ref. 6, confirming this theory. A silicon enriched barrier around $NaLaF_4$ nano-crystals was also discerned from an Electron Energy Loss spectroscopy (EELS) line scan in ref. 7. Thus, the formation of growth inhibiting barriers seems to be a common feature in oxyfluoride systems.

In a previous work we reported on the precipitation of LaF_3 nanocrystals having diameters of approximately 20 nm in a glass of composition $55SiO_2$–$20Al_2O_3$–$15Na_2O$–$10LaF_3$ (mol%), in which around 7.3 wt% (2.5 mol%) of LaF_3 crystallizes after a thermal treatment of 620 °C during 40 h.[8] TEM and EDXS analysis indicated that the parent glass possesses nano-sized phase-separated regions, containing La and F but also silicon and oxygen in addition to traces of Al. On annealing, LaF_3 nano-crystals form, which are trapped in a volume determined by the size of the preceding liquid–liquid phase-separation droplets. The remaining volume of these former droplets is filled with the excess of Si, Al, and O. Diffusion barriers and the confinement to the de-mixed ranges in which fluoride crystallizes are assumed to freeze the crystal growth at crystal sizes smaller than de-mixed droplets.

The effect on macroscopic properties of the addition of 1 mol% Tm_2O_3 to the above-mentioned base glass composition has been reported in ref. 1. Tm^{3+} ions provide interesting optical properties to the glass, like blue up-conversion emission from the excitation in the near infrared range. The same crystallization mechanism, involving on the one hand La- and F-enriched phase-separation droplets in the parent glass as precursors of LaF_3 nano-crystals, and on the other hand the deceleration of the crystal growth velocity, is observed for the Tm-doped composition as well. It is reported that the addition of Tm_2O_3 delays the crystallization process in comparison with the un-doped composition. Additionally, Tm_2O_3 seems to contribute to fluorine retention, leading to a phase separation that is more extended, in comparison with the Tm^{3+}-free glass. Optical characterization of the Tm^{3+}-doped glasses and glass-ceramics is reported in ref. 1. The results thereof evidence the partial distribution of Tm^{3+} ions in the LaF_3 nano-crystals in the glass-ceramics, showing a blue up-conversion emission more intense in the glass-ceramic compared with that of the parent glass. However, in literature,

[a]*Fraunhofer Institute for Mechanics of Materials IWM, Walter-Huelse-Straße 1, 06120 Halle, Germany. E-mail: araceli.pablos-martin@iwmh.fraunhofer.de*
[b]*Instituto de Cerámica y Vidrio (CSIC), C/Kelsen 5, Campus de Cantoblanco, 28049 Madrid, Spain*

the verification of the incorporation of RE ions in nanocrystalline phases in glass-ceramics is mainly based on optical techniques, such as luminescence spectroscopy and luminescence decay curves.[9,10] Tikhomirov *et al.*[9] reported glass-ceramics of composition $32SiO_2$–$9AlO_{1.5}$–$31.5CdF_2$–$18.5PbF_2$–$5.5ZnF_2$:$3.5REF_3$, mol%, where RE are Yb^{3+}–Er^{3+} co-dopants, in which PbF_2 crystallises. The down-conversion efficiency is analysed. Lahoz *et al.*[10] reported a glass of similar composition $30SiO_2$–$15Al_2O_3$–$29CdF_2$–$22PbF_2$–$(4 - x - y)YF_3$–$xTmF_3$–$yYbF_3$, with x = 0, 0.1, and 1 and y = 0 and 2.5. They studied the blue up-conversion emission under the excitation in the near infrared. As an exception of works based in optical techniques to confirm the inclusion of RE ions in the crystalline phase, Yu *et al.*[11] proposed a mechanism to describe the distribution of Nd^{3+} ions between PbF_2 nanocrystals and the glassy matrix through energy dispersive X-ray spectroscopy (EDS) simulations.

To study the nanostructure of glasses and glass-ceramics, transmission electron microscopy (TEM) has proved to be a very useful technique.[12] In particular, it has been successfully used to detect and characterize phase separation phenomena in oxyfluoride glasses.[13]

In the past decade, aberration correction and new detectors became available, constituting the new generation of transmission electron microscopes. Aberration correction facilitates imaging and analytics at much reduced acceleration voltages (80 or even 60 keV instead of 300 keV) while still keeping a spatial resolution unsurpassed by other techniques. Low acceleration voltages are particularly favorable to reduce radiation damage of electron-beam sensitive oxyfluoride glasses.[14]

To the best of our knowledge, to date, no studies exist concerning the particular distribution of RE ions in oxyfluoride glass-ceramics, based on TEM techniques. However, the possibility to perform elemental distribution mappings of RE elements would allow to directly localizing RE ions in the glass and glass-ceramics. Thus, the aim of this work is to complete our previous studies,[1] thus adding unexcelled spatial resolution by using TEM and Energy Dispersive X-Ray Spectroscopy (EDXS) techniques complementing the rather integral techniques used before.

Moreover, the present work provides new features concerning the compositional gradients surrounding nano-sized phase-separation droplets and the corresponding nano-crystals, completing the previously suggested crystallization mechanism.

Materials and methods

A glass of nominal composition $55SiO_2$–$20Al_2O_3$–$15Na_2O$–$10LaF_3$ (mol%) doped with 1 mol% Tm_2O_3 was prepared by melting reagent grade SiO_2 (Saint Gobain, 99.6%), Al_2O_3 (Panreac), Na_2CO_3 (Panreac, 99.5%), LaF_3 (Panreac, 99%) and Tm_2O_3 (GFS Chemicals, 99.9%), in an electric furnace. The batch was first calcined for two hours at 1200 °C and then melted at 1600 °C for 1.5 h. The melts were quenched twice in air onto a brass mould in order to obtain homogeneous transparent glasses, which were then annealed at T_g +5 °C for 30 min. The glass-ceramic was obtained after heat treatment at 620 °C for 40 h.[1] The complete chemical, thermal and structural characterization of the glass and glass-ceramic was reported in ref. 1.

TEM preparation of glass and glass-ceramics samples was done as follows: in a first step, the samples were prepared by cutting slices, plane-parallel grinding, and dimpling to a residual thickness of ~10–15 μm. Then double-sided ion-beam milling using low-energy (2.5 keV) Ar^+ ions under small angle of incidence ($\pm 5°$) was applied until the central part of the samples became electron transparent (precision ion-polishing system PIPS, Gatan Company). The non-conducting samples were area-selectively coated with carbon on both sides, using a special coating mask[15] prior to TEM investigation in order to reduce charging effects associated to the interaction with the electron beam.

The TEM analysis of the samples was done on an FEI Titan^3 80–300 electron microscope (FEI Company). All the samples proved to react very sensitively to the electron beam in terms of degradation, so the acceleration voltage was reduced from 300 kV to 80 kV in order to minimize the sample damage.

For the analysis of delicate samples, scanning transmission electron microscopy (STEM) can have certain advantages over TEM (*i.e.*, illumination of the sample with a parallel electron beam, rather than with a fine-focused probe). First, the electron dose is lower in STEM, which can be crucial for electron-sensitive samples. Second, it offers improved spatially resolved analytics in terms of a fine spot for imaging in combination with energy-dispersive X-ray spectroscopy (EDXS).[13] Thus, besides TEM analysis, STEM with a high-angle annular dark-field (HAADF) detector (Fischione model 3000, camera length: 145 mm, Fischione Company) was performed on the samples as well, using the same electron microscope. In combination with energy dispersive X-ray spectroscopy (EDXS) by means of a Super X-EDXS detector (FEI Company) that consists of four silicon drift detectors, thus offering a maximum collection angle of 0.9 sr above the sample surface, elemental mappings of different elements were obtained, in order to gain information about the elemental distribution with high spatial resolution.

Line scans and elemental mappings were obtained by evaluating the peak intensity, that is, the area under either the K_α- (O, F, Na, Al, Si) or L_α- (La, Tm) edges of the respective elements, with an automatic routine provided by the commercially available software Esprit1.8 (Bruker Company). A change of the Tm signal intensity between crystal and glassy matrix, and, therefore, a higher Tm content in the crystal can qualitatively be determined. Experimental conditions were improved to get the best signal/noise ratio in the glass and glass-ceramic. For the line scan in the glass, it was found that 3 minutes of acquisition time provide the best EDXS spectrum avoiding damage, while for the glass-ceramic, that proved to be more stable concerning electron-beam-induced sample

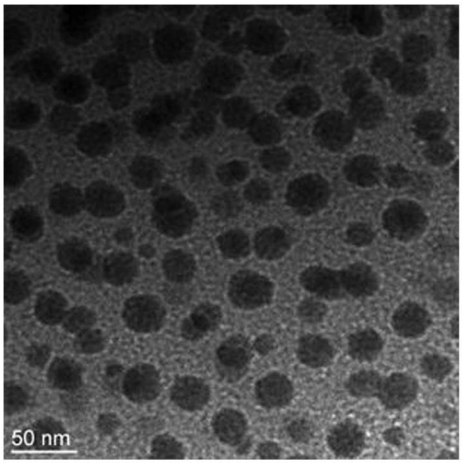

Fig. 1 Bright field micrograph of the glass.

damage, the acquisition time could be prolonged until 10 min, giving a less noisy spectrum with respect to that of the glass.

Most of the experiments were carried out at room temperature with a conventional double-tilt TEM sample holder (FEI Company); however, one experiment was performed with a special Cryo-Transfer Holder (model 915 Gatan Company), in which the sample was kept at liquid-nitrogen temperature, in an attempt to minimized the radiation damage due to the mobility of high diffusivity ions like Na.

Results and discussions

Tm-doped parent glass

The bright-field micrograph of the glass shown in Fig. 1 clearly shows the phase-separated La-enriched region as droplets with diameters of around 30–40 nm. As previously reported in ref. 1, the size distribution of the droplets is quite homogeneous.

Fig. 2a shows a STEM micrograph of this glass. The compositional profile obtained from an EDXS line scan across a phase-separation droplet (indicated with a yellow arrow in the figure) is shown in Fig. 2b. Apparently, the La- and F-concentrations greatly increase within the phase-separation droplet in comparison to the surrounding matrix. A shift of the fluorine signal from the center of the droplet is observed. This is an indication of an uneven fluorine distribution within the droplet. It was previously reported in ref. 8 that up to four crystallites can crystallize within the volume of a droplet, so the fluorine distribution observed in the phase-separated glass may anticipate this non-homogeneous LaF_3 precipitation. Moreover, it is observed that the Si signal intensity decreases towards the center of the droplet. Additionally, there is evidence that the Al signal intensity increases at the outer ring of the separation droplets respecting to the very center of them. This indicates that a thin shell-like structure (of approximately 5 nm) that surrounds the droplet is enriched in Al.[6] On the other hand, Si intensity decreases in the center of the droplets but increases significantly in the surroundings, forming a SiO_2-enriched shell of around 35 nm around the

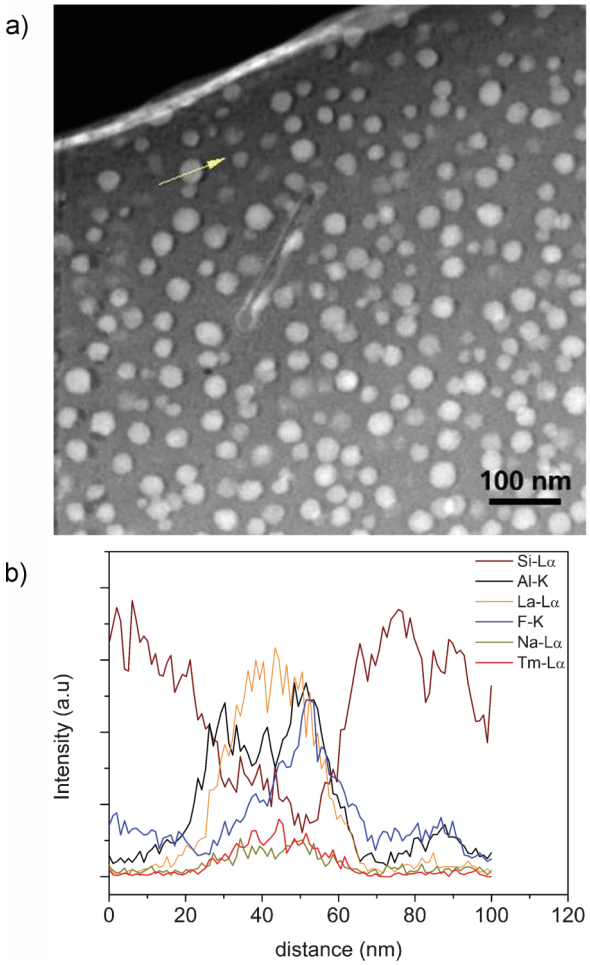

Fig. 2 (a) Dark field STEM image (annual dark-field detector) with the location of spot analysis indicated as a yellow arrow. The line crossing two nano crystals close to the yellow arrow corresponds to the radiation trace after recording a previous EDX line scan. (b) EDX Line Scan along the trace of the line scan indicated in (a).

Al_2O_3 thin crown. In ref. 8 it was stated that the phase separation droplets contain lanthanum, silicon, oxygen, together with traces of aluminum.

Thanks to the improvement of spatially resolved analytics in these STEM/EDXS measurements, the present work goes further, evidencing that Al is in fact forming a first thin shell surrounding the droplets. Besides the observed enrichment of La and F in the phase separation droplets, the EDXS line scan shown in Fig. 2b additionally gives the impression that the Na signal increases as well in the area where the droplets are located. However, the diffusion or loss of alkali cations due to the beam damage in TEM experiments can produce a significant effect which may give rise to serious errors in TEM analyses, as pointed out in previous studies[16] and will be discussed later on in this work. Ahn *et al.*[16] (and references therein) reported the radiation damage in Na-containing micas under the TEM electron beam. They observed an intensity decrease in the Na-EDX peak after 100 s exposure time, due to the Na diffusion from the thin areas of the

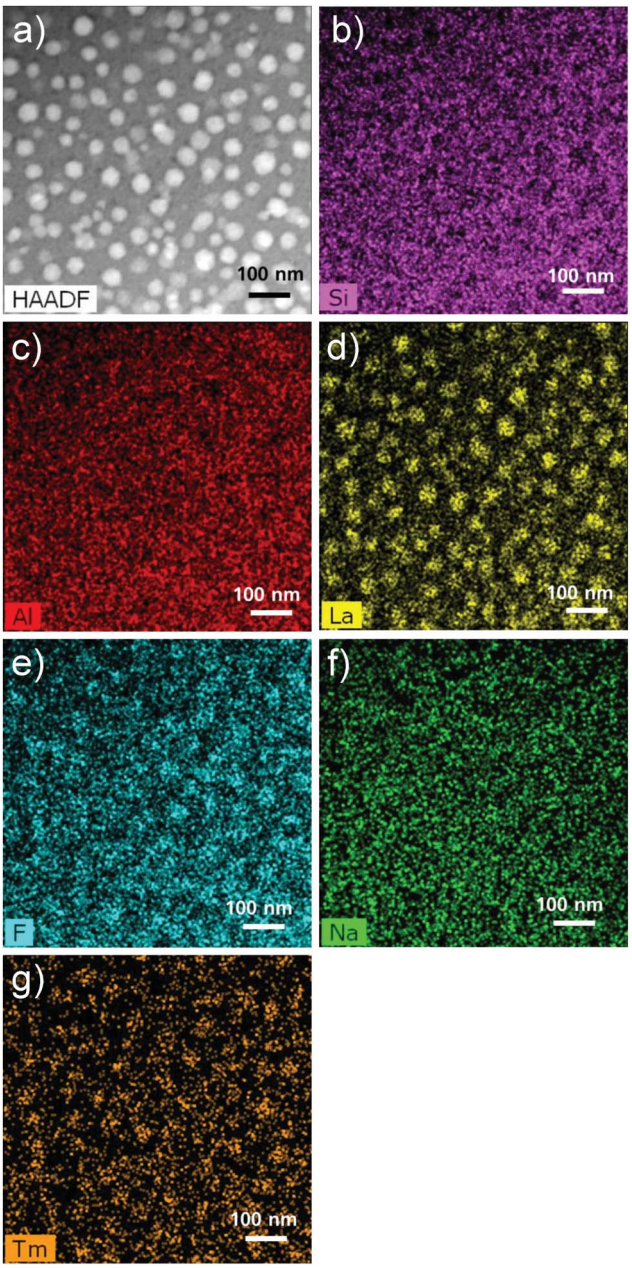

Fig. 3 (a) HAADF micrographs taken in STEM mode of the glass and the corresponding EDXS mappings of (b) Si, (c) Al, (d) La, (e) F, (f) Na, (g) Tm.

sample, which gives rise to fissures. Thus, the distribution of Na reported in this work cannot be totally confirmed, since the beam-induced diffusion of Na could be an artifact that influences the measurement results.

Finally, with the EDXS line scan it is also observed that the Tm concentration increases in the phase separation droplet area.

Fig. 3 shows a STEM micrograph and the corresponding EDXS analyses presented as lateral elemental distribution maps. By comparing the HAADF STEM image (Fig. 3a) with the corresponding elemental maps (Fig. 3b–3g), some conclusions can be drawn, which provide new information on the nature of the phase separation droplets, in comparison to previous work.[1,8]

First, the mappings indicate that Si (Fig. 3b) and Al (Fig. 3c) are distributed over the whole glassy matrix, although a light depletion of these elements is observed in the center of the droplets, in agreement with the EDXS line scan (Fig. 2b).

The phase-separation droplets certainly contain La (Fig. 3d) and F (Fig. 3e), as expected from previous works.[1] La is highly concentrated in the phase-separation droplets, although a small quantity remains in the rest of the glassy matrix. Fluorine is found both in the phase separation droplets as well as in the matrix (Fig. 3e). This F distribution agrees with the ^{19}F NMR data from this glass reported in ref. 17, in which it is stated that fluorine is distributed between La–F and Al–F–Na bonds.

Fig. 3f shows the Na map of the glass. As previously mentioned, the measurement of Na is affected by its extremely diffusion rate under the electron beam and the resulting map is not reliable.

Additionally, the Tm map in Fig. 3g clearly shows that Tm is incorporated and enriched in the amorphous phase-separation droplets, although there is still a significant Tm-content in the matrix. At this point, it is worth mentioning that the possibility of actually being able to map the distribution of as little as less than 1 mol% of Tm (with respect to the other elements that the sample consists of) in a radiation sensitive sample is a very difficult task and has been successfully carried out. It is only possible through a combination of proper sample preparation, cutting-edge analytical transmission electron microscopy at reduced acceleration voltage and, particularly, the application of an EDXS detector system such as the one used for the experiments here.

The location of Tm in the phase-separation droplets jointly with La agrees with the similitude between the lanthanides radii. In ref. 1 it was reported that the addition of Tm_2O_3 increases the extension of the phase separation, in comparison with the un-doped glass, leading to the increase of T_g. Moreover, from the optical point of view, this F-enriched environment around Tm (*i.e.*, the phase-separation droplets) already in the glass, explains an up-conversion emission that is only slightly less intense to that of the glass-ceramic reported in ref. 1.

Tm-doped glass-ceramic

During the annealing of the parent glass at 620 °C for 40 h, LaF_3 crystallizes,[1] as illustrated by Fig. 4a which shows a bright field TEM micrograph of this glass-ceramics. As previously reported, LaF_3 nano-crystals precipitated in a residual glassy matrix, with a homogenous size distribution (crystal diameters of *ca.* 10–20 nm). The crystallites are smaller than the preceding droplets. Indeed, up to four crystallites have been observed within the volume of a former droplet.[8] The crystal size distribution is quite narrow. Due to the sensitivity of the samples under the electron beam, some damaged areas around the LaF_3 nano-crystals, corresponding to brighter features in the images, are observed after irradiation lasting some 10 s. This particular location of the damaged areas in the periphery of the crystals was previously observed in $NaLaF_4$-glass-ceramics.[7] This damage also suggests some chemical

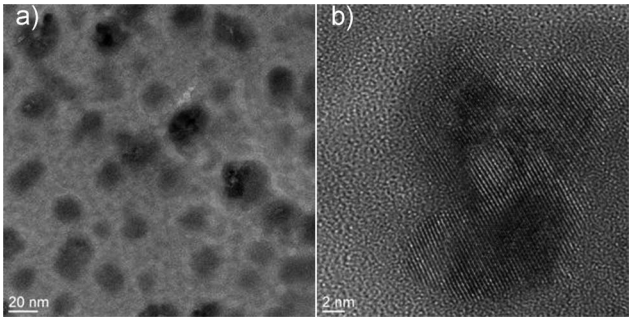

Fig. 4 (a) Bright field micrograph of the glass-ceramic after annealing at 640 °C for 40 h. (b) High resolution micrograph of a LaF_3 nano-crystal.

peculiarity of the interphases between nano-crystals and matrix, which may be related to the presence of Na, an element of high ion diffusivity, in these areas (Fig. 2b). From ^{19}F NMR (ref. 17) it is known that part of the F atoms must migrate from Al–F–Na bonds to form the LaF_3 nano-crystals.

Fig. 4b shows a high resolution micrograph of one LaF_3 crystal. Lattice planes can be clearly discerned, indicating the single-crystalline character of the nano-crystals.

The crystallization mechanism suggests that the liquid–liquid phase-separation droplets in the glass develop into LaF_3 nano-crystals upon annealing.[1] Fig. 5a shows a STEM micrograph of the glass-ceramic. The dark contrast that partly surrounds some of the crystals corresponds to the damaged areas mentioned above. In order to evaluate the elemental distribution in the glass-ceramic, an EDXS line scan across three nano-crystals (indicated by the green arrow in Fig. 5a) was performed. The results are displayed in Fig. 5b. The La- and F-concentrations greatly increase especially at the position of the first, large nano-crystal in the line scan, thus underlining the precipitation of LaF_3 nano-crystals upon thermal treatment. It can be observed that the Si and Al intensities decrease at the center of the crystalline area of this first crystal, while a slight increase of the signal intensities of both elements is observed in the periphery of the crystal. From the positions where the La-, F- and Al-signals increase, the size of this crystal is 20 nm, smaller than the *ca.* 30 nm size of the phase separation droplet from Fig. 2b. The remaining volume is filled with Al. In fact, the Al line scan exhibits two well defined peaks at the edges of the first crystal in the line scan, constituting an Al-enriched shell of 7–10 nm thickness in the periphery of the crystal. The formation of Al-enriched shells was previously reported in ref. 14, where an alumina layer grows around the $ZrTiO_4$ nucleants in lithium aluminosilicate glasses. The glassy matrix around the crystal is enriched in silicon, already present in the phase separation droplets in the parent glass (Fig. 2b and 3b). It was previously reported that this enrichment in silicon greatly increases the viscosity in this area, leading to the inhibition of further crystal growth.[1,8]

The fact that the increase of the Na- and F-signal intensities is not so pronounced for the second and third crystal in the line scan in Fig. 5b likely indicates that these crystals, that appear smaller in the STEM micrograph than the first one, were detached during the sample preparation, and only the Al

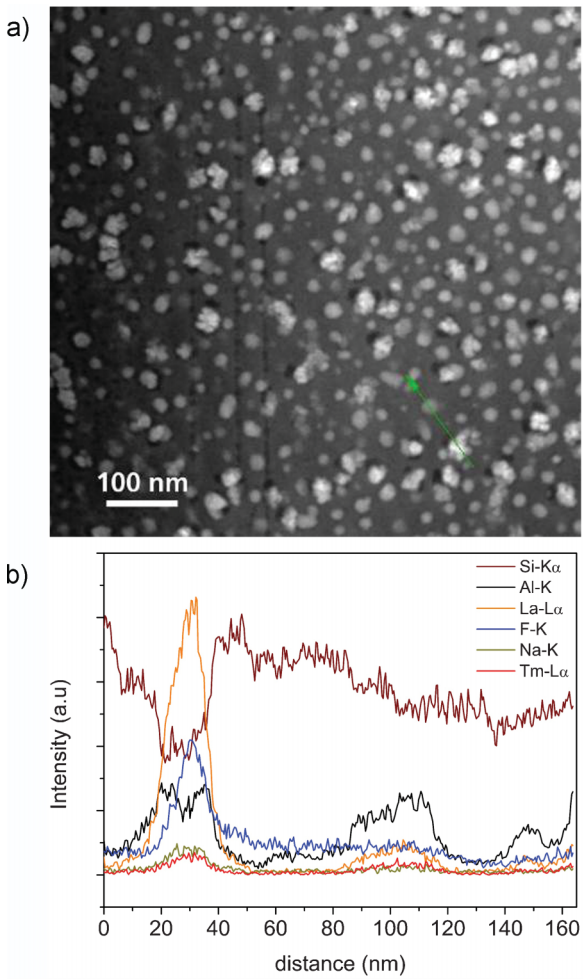

Fig. 5 (a) Dark field STEM image (annual dark-field detector) of the glass-ceramic after annealing at 640 °C for 40 h with the location of spot analysis indicated as a green arrow. (b) EDX Line Scan along the trace of the line scan indicated in (a).

crown formed around them is visible in the line scan. In contrast, it is believed that the first nanocrystal in the line scan is fully incorporated in the sample volume.

In the line scan, it is also observed that the Tm concentration increases in the crystalline areas, evidencing the location of these optically active ions in the LaF_3 structure. This enrichment of Tm^{3+} ions in the LaF_3 crystalline structure enhances the up-conversion emission of the glass-ceramic, compared with that in the glass, as shown in ref. 1.

Again, as mentioned in the previous section, the Na elemental distribution is difficult to interpret. Thus, in order to go deeper into this subject, STEM experiments were done using a cryo-TEM holder at liquid N_2 temperature (−185 °C), with the aim to keep the Na mobility as low as possible. Fig. 6a shows a STEM micrograph of the glass-ceramic that was taken just after scanning the electron beam over an area in the middle of this micrograph for 5 min, which was done to accumulate current in this region in an attempt to mimic severe radiation-induced sample damage. The extent of the radiation damage in the sample can be clearly observed: the

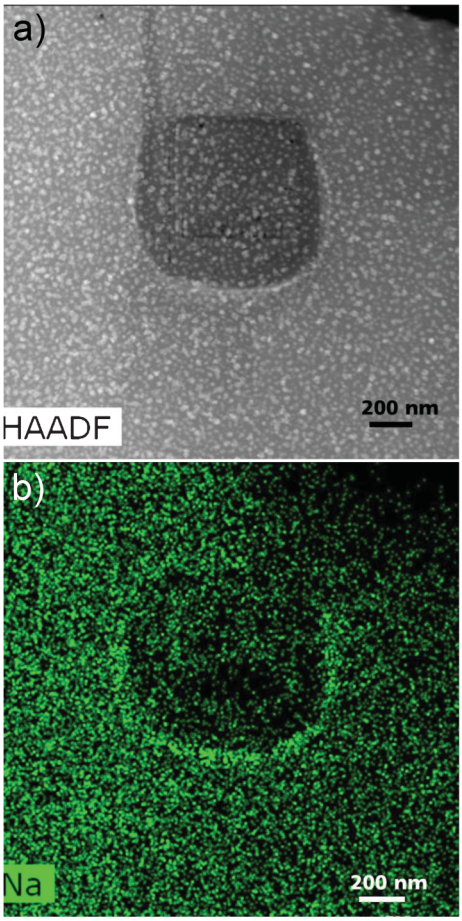

Fig. 6 (a) HAADF micrograph taken in STEM mode of the glass-ceramic after annealing at 640 °C for 40 h and the corresponding EDXS Na-mapping (b), recorded with the cooling holder.

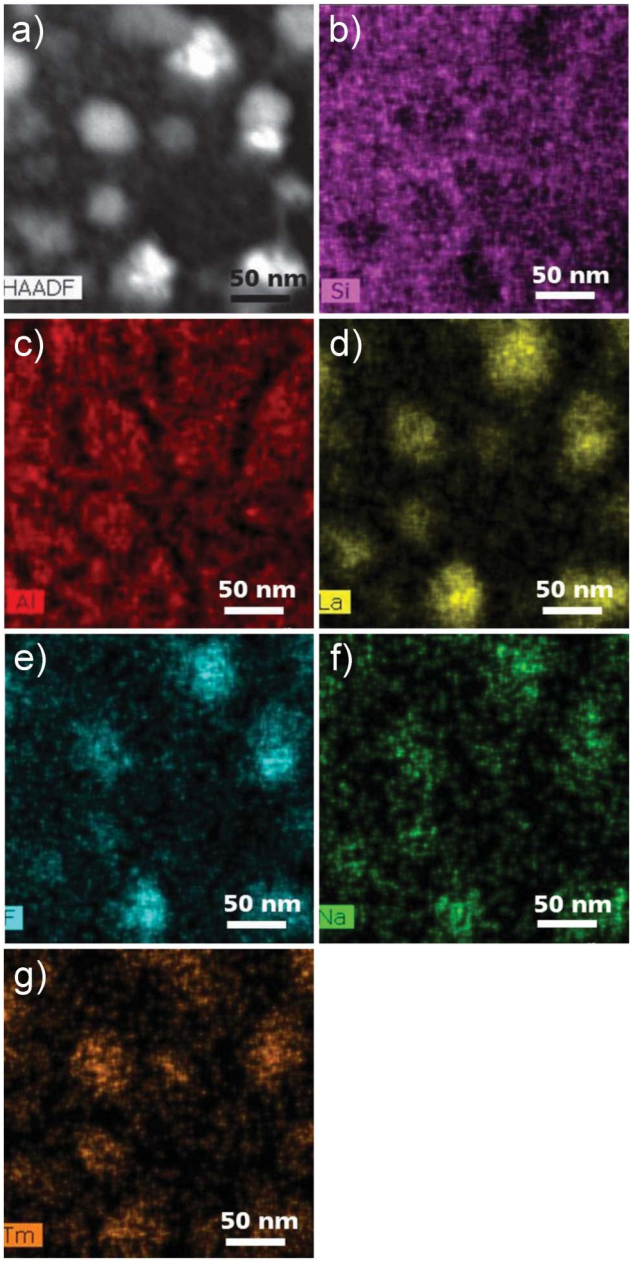

Fig. 7 (a) HAADF micrographs taken in STEM mode of the glass-ceramic after annealing at 640 °C for 40 h and the corresponding EDXS mappings of (b) Si, (c) Al, (d) La, (e) F, (f) Na, (g) Tm.

dark contrast in the center of Fig. 6a marks the area at which the first STEM micrograph was taken, indicating the structural change of this area in comparison to its surrounding. Fig. 6b shows the corresponding Na element distribution map. It is observable even at liquid-nitrogen temperature. Na has clearly diffused from the center of the scanned area towards the periphery of the latter, where an enhancement of Na is observed. This Na diffusion must be taken into consideration when interpreting the elemental maps which have been discussed above, and the Na measurement might be a result of beam-induced Na diffusion.

Similarly to the glass, EDXS elemental mappings were also acquired for the glass-ceramics (Fig. 7a). Si (Fig. 7b) clearly occupying the residual glassy matrix. Si is depleted in the center of the crystalline areas, while the edges of the crystal agglomerates are enriched in this element, in agreement with the EDXS line scan shown in Fig. 5b. Al (Fig. 7c) is distributed across the entire area analyzed, but some enrichment of this element can be observed at the periphery of the crystals, forming the above-mentioned first shell. The mappings prove that the crystals contain La and F (Fig. 7d and 7e). Fig. 7f shows the Na map in this glass-ceramic. Taking into account the radiation damage observed in Fig. 6, the distribution of Na in this glass-ceramic will not be considered in closed detail.

Tm (Fig. 7g) is enriched in the LaF_3 crystals, but some thulium remains in the glassy matrix, which, as previously mentioned, is very relevant from the optical point of view, and is in good agreement with our previous results.[1]

Concluding from these results and those in ref. 1 the crystallization mechanism can be described more precisely according with the sketch given in Fig. 8: the parent glass contains La- and F-enriched phase separation droplets, also containing Si-, Al- and O. The doping ion Tm^{3+} is partly incorporated in the phase-separation regions. Al is present,

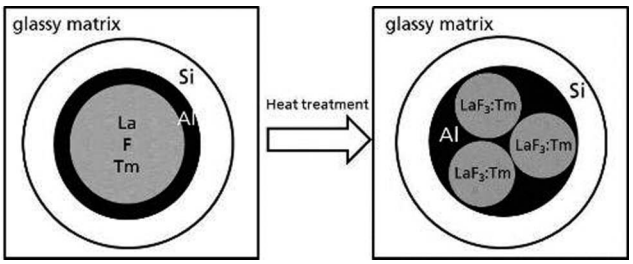

Fig. 8 Scheme of the nano-crystallisation mechanism in the studied Tm^{3+} doped glass.

likely as Al_2O_3, in a thin shell surrounding the droplets. Upon annealing, the growth of the LaF_3:Tm crystallites within these phase separation droplets takes place.

Conclusions

Based on previous works, the proposed mechanism for the LaF_3 nano-crystallisation in Tm_2O_3 doped-oxyfluoride glass-ceramic has been modified and improved by using HR-TEM and EDX techniques.

The parent glass is constituted by *ca.* 30 nm amorphous phase separation regions containing La and F. The dopant ion Tm^{3+} is partially included in both, the glass matrix and the phase separation droplets. The near surrounding of the droplets is enriched in Al and Si.

After the heat treatment of the parent glass, the La-, F-, Tm-enriched droplets develop LaF_3 nano-crystals, which act as main host for the Tm^{3+} ions. Thanks to the advanced STEM/EDSX analysis, it was possible to identify a thin Al enriched layer around the crystals, and a second shell enriched in Si, both inhibiting further crystal growth, enabling the nano-crystal size.

Additionally, the verification of the incorporation of Tm^{3+} ions in the LaF_3 nanocrystals through EDX elemental mappings is a great advance in the understanding of rare earth doped glass-ceramics, since it is the key feature of these materials for their application in optical devices.

Acknowledgements

The authors acknowledge the financial support of the project MAT2010-20459 of Spanish Government and the FhG Internal Programs under Grant No. Attract 692 280.

References

1 A. de Pablos-Martín, D. Ristic, S. Bhattacharyya, T. Höche, G. C. Mather, M. O. Ramírez, S. Soria, M. Ferrari, G. C. Righini, L. E. Bausá, A. Durán and M. J. Pascual, *J. Am. Ceram. Soc.*, 2013, **96**, 447–457.
2 A. de Pablos-Martin, M. O. Ramirez, A. Duran, L. E. Bausa and M. J. Pascual, *Opt. Mater.*, 2010, **33**, 180–185.
3 G. Dominiak-Dzik, R. Lisiecki, W. Ryba-Romanowski and L. Krajczyk, *J. Alloys Compd.*, 2012, **511**, 189–194.
4 A. de Pablos-Martin, A. Duran and M. J. Pascual, *Int. Mater. Rev.*, 2012, **57**, 165–186.
5 C. Rüssel, *Chem. Mater.*, 2005, **17**, 5843–5847.
6 S. Bhattacharyya, C. Bocker, T. Heil, J. R. Jinschek, T. Höche, C. Rüssel and H. Kohl, *Nano Lett.*, 2009, **9**, 2493–2496.
7 A. de Pablos-Martin, G. C. Mather, F. Munoz, S. Bhattacharyya, T. Höche, J. R. Jinschek, T. Heil, A. Duran and M. J. Pascual, *J. Non-Cryst. Solids*, 2010, **356**, 3071–3079.
8 A. de Pablos-Martin, N. Hemono, G. C. Mather, S. Bhattacharyya, T. Höche, H. Bornhoft, J. Deubener, F. Munoz, A. Duran and M. J. Pascual, *J. Am. Ceram. Soc.*, 2011, **94**, 2420–2428.
9 V. K. Tikhomirov, V. D. Rodríguez, J. Méndez-Ramos, J. Del-Castillo, D. Kirilenko, G. Van Tendeloo and V. V. Moshchalkov, *Sol. Energy Mater. Sol. Cells*, 2012, **100**, 209–215.
10 F. Lahoz, I. R. Martin, J. Mendez-Ramos and P. Nunez, *J. Chem. Phys.*, 2004, **120**, 6180–6190.
11 H. Yu, H. Guo, M. Zhang, Y. Liu, M. Liu and L.-j. Zhao, *Nanoscale Res. Lett.*, 2012, **7**, 1–7.
12 T. Höche, *J. Mater. Sci.*, 2010, **45**, 3683–3696.
13 S. Bhattacharyya, T. Höche, K. Hahn and P. A. van Aken, *J. Non-Cryst. Solids*, 2009, **355**, 393–396.
14 S. Bhattacharyya, T. Höche, J. R. Jinschek, I. Avramov, R. Wurth, M. Müller and C. Rüssel, *Cryst. Growth Des.*, 2010, **10**, 379–385.
15 T. Höche, J. W. Gerlach and T. Petsch, *Ultramicroscopy*, 2006, **106**, 981–985.
16 J. H. Ahn, D. R. Peacor and E. J. Essene, *Ultramicroscopy*, 1986, **19**, 375–381.
17 F. Munoz, A. de Pablos-Martin, N. Hemono, M. J. Pascual, A. Duran, L. Delevoye and L. Montagne, *J. Non-Cryst. Solids*, 2011, **357**, 1463–1468.